Phasor-based single-molecule fluorescence lifetime imaging using a wide-field photon-counting detector

R. Colyer[1], O. Siegmund[2], A. Tremsin[2], J. Vallerga[2], S. Weiss[1], X. Michalet[1*]

[1]Department of Chemistry & Biochemistry, UCLA, Los Angeles, CA
[2]Space Sciences Laboratory, UCB, Berkeley, CA

ABSTRACT

Fluorescence lifetime imaging (FLIM) is a powerful approach to studying the immediate environment of molecules. For example, it is used in biology to study changes in the chemical environment, or to study binding processes, aggregation, and conformational changes by measuring Förster resonance energy transfer (FRET) between donor and acceptor fluorophores. FLIM can be acquired by time-domain measurements (time-correlated single-photon counting) or frequency-domain measurements (with PMT modulation or digital frequency domain acquisition) in a confocal setup, or with wide-field systems (using time-gated cameras). In the best cases, the resulting data is analyzed in terms of multicomponent fluorescence lifetime decays with demanding requirements in terms of signal level (and therefore limited frame rate). Recently, the phasor approach has been proposed as a powerful alternative for fluorescence lifetime analysis of FLIM, ensemble, and single-molecule experiments. Here we discuss the advantages of combining phasor analysis with a new type of FLIM acquisition hardware presented previously, consisting of a high temporal and spatial resolution wide-field single-photon counting device (the H33D detector). Experimental data with live cells and quantum dots will be presented as an illustration of this new approach.

Keywords:

FLIM, TCSPC, phasor, single-molecule, quantum dot, fluorescence lifetime, single-photon counting, wide-field detector

1 INTRODUCTION

Fluorescence lifetime imaging (FLIM) is rapidly increasing in popularity for biological research, as new hardware and new analysis techniques are making it more accessible. It is used for measurements of the ratios of fluorophores in a region, or for concentration-independent measurements of various changes to the chemical environment such as ion concentration, binding processes, or proximity between a donor and acceptor in the case of Förster resonance energy transfer (FRET)[2, 3].

In confocal systems, raster scanning acquisition using PMTs or APDs with time-correlated single photon counting (TCSPC)[4] or digital frequency domain (DFD)[5] hardware is used to provide high sensitivity lifetime measurements suitable for single molecule imaging. In wide-field systems, time-gated acquisition or homodyned camera systems can be used to provide lifetime images at video-rates, although with a substantial loss of sensitivity due to the discarding of photons[6]. However, there are many rapid biological processes, such as in neuronal signaling, which could be studied in greater depth using a wide-field high-sensitivity FLIM system capable of observing processes at video-rates or faster. The field currently lacks such a system, but we present a proof-of-concept prototype, shown previously[1, 7], and we show how the principle of operation can be advanced to provide a wide-field high-sensitivity high-throughput FLIM system.

Lifetime data is typically acquired as a histogram of nanotime values. For a conventional time-domain analysis, this data is then fit to one or more exponentials convolved with an instrument response function (IRF). This process can be

* To whom correspondence should be addressed: michalet@chem.ucla.edu

Single Molecule Spectroscopy and Imaging II, edited by Jörg Enderlein, Zygmunt K. Gryczynski, Rainer Erdmann
Proc. of SPIE Vol. 7185, 71850T · © 2009 SPIE · CCC code: 1605-7422/09/$18 · doi: 10.1117/12.809496

computationally slow, requires initial guesses which can be complicated and difficult to interpret in the case of multiexponential systems, as is commonly found in a cellular environment[8]. Because of these problems, phasor analysis has recently been growing in popularity as a more convenient approach to lifetime analysis[9-11]. The calculation of phasors is extremely rapid, is a simple transformation of the data requiring no initial guesses, and handles multiexponential systems seamlessly[12].

Recent developments with phasor analysis for the representation and analysis of lifetime images have resulted in a substantial increase in the accessibility and rigor of lifetime analysis. In the phasor approach, a rapid Fourier analysis translates lifetime information into a graphical representation called the phasor plot, in which lifetime differences across various regions of the image can be easily distinguished. We will show that the algorithms of phasor analysis integrate quite naturally with the architecture of our H33D detector, and that by combining these two approaches we gain substantial advantages in data analysis and interpretation.

2 MATERIAL AND METHODS

2.1 Sample

Cells: The sample preparation was previously described in ref. [1]. Briefly, quantum dots (qdots) emitting at 620 nm and coated with non-biotinylated peptides were targeted to HeLa cells that stably express a glycosylphosphatidylinositol (GPI)-anchored avidin (GPI-av)[13] and caveolin 1-EGFP (Cav1-EGFP). For imaging, HeLa cells were grown in DMEM media supplemented with 5 % fetal calf serum (FCS) on fibronectin coated temperature-regulated wells (SmartSlide 100, Wavergen, Fremont, CA). Cells were kept at 37 °C through all labeling steps and during imaging. Cells were pre-incubated in a HBSS + 1% BSA buffer for 10 min before the addition of 10 nM qdots. Qdots were incubated overnight with HeLa cells, resulting in non-specific endocytosis. Cells were then rinsed with DMEM medium and imaged at 37 °C.

Beads: 220 nm diameter nile red fluorescent beads (Invitrogen): excitation peak: 535 nm/emission peak: 575 nm where diluted 100 times in Tris-EDTA buffer, sonicated for 5 min and centrifugated at 14,000 rcf (relative centrifugal force). 10 µl of the supernatant were spin cast on cleaned glass coverslip (4,000 rpm) before observation.

Single quantum dots: 5 mg of 577 nm emitting CdSe/ZnS core shell quantum dot power (Ocean Nanotech, Springdale, AR) were diluted in 1 ml butanol. After 2 successive 100 times dilution in butanol, 10 µl of the sample were spin cast on cleaned glass coverslip (4,000 rpm) before observation.

2.2 Experimental Setup

The experimental setup used in these experiments has already been described[7]. Briefly, the sample was excited using either of the two following laser sources. For live-cell imaging, the output of a 76 MHz pulsed femtosecond Ti:Sa laser (Mira 900, Coherent, Santa Clara, CA) pumped by an Argon ion laser (Sabre, Coherent) was slowed down to a 4.75 MHz repetition rate using a pulse-picker (Model 9200, Coherent) and frequency-doubled using a BBO crystal (Casix, Mountain Lakes, NJ). The resulting 442 nm pulsed light was expanded and focused on the back focal plane of a high numerical aperture objective lens of an inverted wide-field microscope (IX 71, Olympus, Center Valley, PA) to obtain epifluorescence illumination of the sample. For single quantum dot and bead imaging, a picosecond-pulsed 532 nm laser beam (IC-532-1000, High Q Laser, Watertown, MA) was coupled to a single-mode fiber and injected into the total internal reflection (TIR) illumination port of the microscope (Olympus).

In both cases, wide-field fluorescence emission was collected using appropriate dichroic mirrors and emission filters, and imaged onto the H33D detector.

2.3 The H33D detector

The H33D detector (pronounced “heed” or High spatial, High temporal resolution, High throughput 3D[†] detector) is a time-resolved wide-field single-photon counting device, which we have previously described[7, 14-16]. We have recently

[†] 3D = 2 spatial and 1 temporal dimension

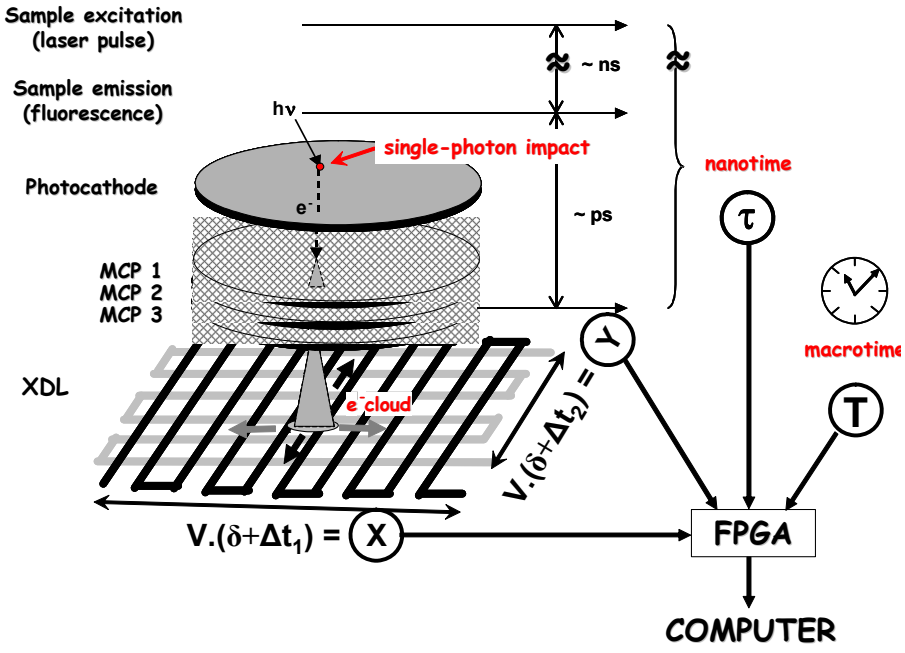

Fig. 1: Principle of the H33D detector. Each photon is converted by the photocathode into a photoelectron amplified ~10^7 times by the MCP stack. The time interval between the pulse generated at the back of the MCP and the laser pulse (nanotime τ) is measured by a TDC. The electron cloud is collected by a cross-delay line anode and a timing electronics module converts the differences in charge arrival time at both ends of the delay lines into position information (X, Y). A laser pulse counter built in the readout electronics provides a 4th coordinate, the macrotime T, which is associated with the 3 other coordinates by a dedicated field-programmable gate array (FPGA), before being sent asynchronously to the computer. δ: fixed time delay. V: velocity factor proportional to the actual anode signal propagation velocity. From ref. [1].

upgraded its readout electronics, but the principle of operation remains identical. Briefly, incoming individual photons first strike a photocathode, generating individual photo-electrons, which are then further amplified by a stack of multichannel plates (MCP) under high voltage. The resulting exiting electron cloud strikes a cross-delay line anode, which is used for the determination of the *x* and *y* coordinates of the incoming photon. This is achieved by measuring the time delay between arrival of the charges at both ends of each delay line using one time-to-digital converter (TDC) per axis (dual-channel TDC model DSTDC-F, Sensor Sciences, Pleasant Hill, CA), as shown in Fig. 1. Each photon's arrival time is determined separately using two different devices. First, coarse timing information (macrotime *T*) is associated with each position by reading out the value of a clock counter (40 MHz, or 25 ns resolution) generated by the field-programmable gate array (FPGA) contained within the dual TDC unit. Second, a precise timing information (nanotime *t*) is obtained by measuring the time separating the MCP output pulse and the next laser pulse using a separate TDC. Both sets of information (*x*, *y*, *T* and *t*) are then associated together, provided they were acquired within a specified timeout window, giving 3-dimensional coordinates for each photon (two spatial and one temporal, the latter being comprised of the two values *T* and *t*).

2.4 Phasor analysis

In phasor analysis of lifetime images, the lifetime data at each pixel is transformed into a coordinate pair called a phasor, and a histogram of the number of pixels with these phasor coordinates is generated called a phasor plot, as shown in Fig 2. These phasor plots show a visual representation of the distribution of lifetime values. By selecting regions of a phasor plot, one can use software to identify regions of an image corresponding to those lifetime values. Alternatively, one can use the phasor values directly to determine quantitative values regarding a pixel, such as a FRET value or the relative intensities of two probes.

A phasor coordinate, written as a *(g, s)* pair, is calculated using a rapid intensity-normalized cosine and sine summation of the nanotime histogram, *H(p)*:

$$g = \frac{1}{N}\sum_{p=0}^{n_p-1}\cos\left(2\pi p / n_p\right)H(p) \tag{2.1}$$

$$s = \frac{1}{N}\sum_{p=0}^{n_p-1}\sin\left(2\pi p / n_p\right)H(p) \tag{2.2}$$

where $\tau = (0, \delta T, \ldots, p\,\delta T, \ldots, (n_p - 1)\,\delta T)$ are the binned time values, $T = n_p\,\delta T = 1/f$ is the phasor period and N is the number of elements in the histogram. The phasor frequency f will be used in the following and is usually taken as an integer fraction of the laser repetition frequency (e.g. 19 MHz = 76 MHz/4 for data in Fig. 6 and 68 MHz for data in Fig. 8 and 9).

The IRF is accounted for in phasor analysis by first relating g and s to their phase (φ) and modulation (m) equivalents,

$$\phi = \tan^{-1}\left(\frac{s}{g}\right) \tag{2.3}$$

$$m = \sqrt{g^2 + s^2} \tag{2.4}$$

and then by taking either a reference measurement with a known lifetime, or measuring the IRF directly. In the case of a measurement with a known lifetime, the phase and modulation of the IRF are determined by inserting both the measured and the "real" expected values of the phase and modulation into the following equations:

$$\phi_{measured} = \phi_{real} + \phi_{IRF} \tag{2.5}$$

$$m_{measured} = m_{real} m_{IRF} \tag{2.6}$$

Then the IRF is accounted for by applying the obtained φ_{IRF} and m_{IRF} to all subsequent measurements to determine the real phasor positions. Note that these reference equations correspond to a simple geometric rotation and scaling transformation on the initial data, and thus they account for the instrument response in a computationally efficient manner.

To analyze the distribution of phasor coordinates in an image, the resulting g and s coordinates are then histogrammed as shown in Fig. 2, yielding a phasor plot. On this plot, single exponential lifetimes are located on the "universal circle" shown as a semicircle around $g = 0.5$, where their lifetime values are given by:

$$\tau = \frac{s}{2\pi f g} \tag{2.7}$$

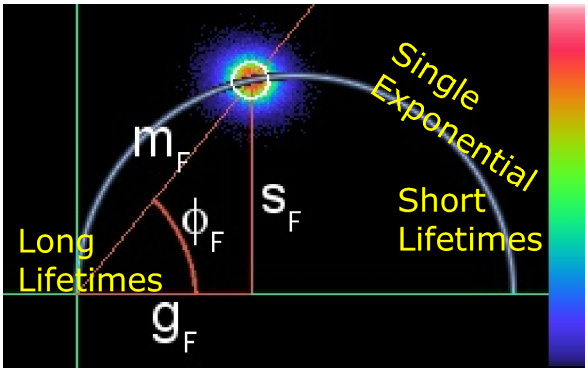

Fig. 2: The structure of a phasor plot is shown. Single exponential lifetimes are located on the semicircle, short lifetimes are located near the bottom right intersection with the x axis, and long lifetimes are located near the origin. The data shown is for a bulk measurement of fluorescein.

Since Eqns. (2.1) and (2.2) are linear, the phasors for multiexponential lifetime decays or combinations of single-exponential lifetime decays are given by the normalized linear combination of the component phasors, making them fall below the universal circle. For instance, combinations of two lifetime components fall on a straight line between the two components, as shown in Fig. 3, with the position along that line given by the relative intensities, according to:

$$g = \sum_i f_i g_i \tag{2.8}$$

$$s = \sum_i f_i s_i \tag{2.9}$$

$$1 = \sum_i f_i \tag{2.10}$$

This linear property of phasors is a valuable tool for the analysis of lifetime images, and in particular, greatly simplifies the analysis of data acquired with the H33D detector, as described below.

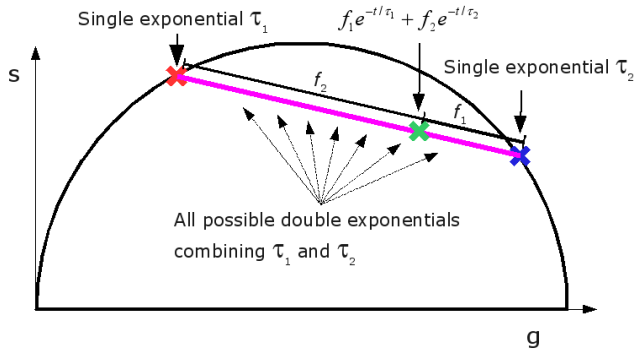

Fig. 3: The linear combination of lifetimes on the phasor plot is demonstrated using the example of adding two single-exponential phasors.

2.5 Phasor ratio images

The phasor plot corresponding to the lifetime information of an image can be used in different ways. The simplest way consists of selecting a region of interest (ROIs) on the phasor plot and highlighting the pixels of the image with phasor values falling within this ROI. Alternatively, in order to visualize the location of all phasor values in the image, some scheme to color code these values can be used. In the particular case where it is known a priori that the sample contains two main species characterized by different phasor values (e.g. a short lifetime species and a long lifetime species), a phasor ratio can be computed for each pixel, which corresponds to the relative contributions of the two components, (g_0, s_0) and (g_1, s_1)[‡]. The phasor ratio of each pixel is computed as follows.
First, the phasor value is projected onto the line connecting the phasor values of the two components. The phasor ratio is obtained as the relative distance of this projected point from the first component (a phasor value projected onto the first component's phasor has a phasor ratio of zero, while a phasor value projected onto the second component's phasor has a phasor ratio of one), as shown in Fig. 4.

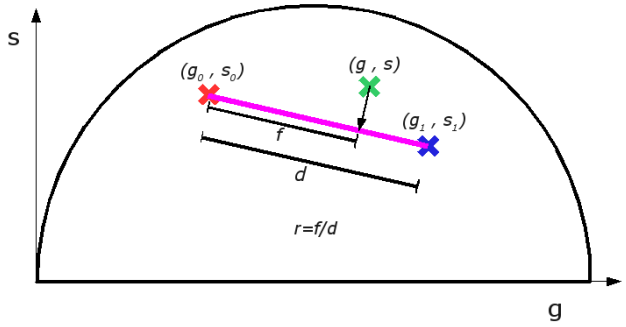

Fig. 4: This schematic shows the geometric projection which is performed to determine the phasor ratio of a point (g, s), showing the relative contributions of two known components, (g_0, s_0) and (g_1, s_1).

‡ Note that the two species do not need to be characterized by a single fluorescence lifetime. What matters is that they each can be represented by a single phasor value.

Practically, the phasor ratio is obtained as follows. First, the angle and scaling factor for the ratio plot are calculated by:

$$\theta = \tan^{-1}\left(\frac{s_1 - s_0}{g_1 - g_0}\right) \tag{2.11}$$

$$d = \sqrt{(s_1 - s_0)^2 + (g_1 - g_0)^2} \tag{2.12}$$

which can be used to yield a rotation matrix:

$$r_g = \cos(\theta)/d \tag{2.13}$$

$$r_s = \sin(\theta)/d \tag{2.14}$$

which in turn produces the phasor ratio value for each pixel:

$$r = (g - g_0)r_g + (s - s_0)r_s \tag{2.15}$$

This phasor ratio value can then be used to determine a color value for each pixel. This calculation uses rapid algebra to produce an image which shows the relative contributions of two single or multi-exponential lifetime components to each pixel in the image, which can be used to provide contrast based on fluorescent species with two different lifetimes, or based on the relative populations of two different FRET states of a FRET construct.

2.6 Data acquisition and analysis

Data acquired by the H33D detector was analyzed using custom software developed using LabView (National Instruments, Austin, TX) and C (Visual Studio 6.0, Microsoft Corp., Seattle; gcc 4.1, GNU/FSF, Boston). This software permits live data display and analysis during acquisition and post-processing of saved raw data.

Typically, since the H33D detector generates a photon stream consisting of (*x, y, t, T*) values, the first task consists of binning this stream temporally based on the macrotime T of each photon, thus defining "frames". The second step consists in the formation of an intensity image corresponding to each frame. Since each coordinate *x* or *y* is encoded on 12 bits (formerly 10 bits, ref. [7]), the image consists of at most 4096 x 4096 "pixels". Each pixel value is equal to the number of photons having these spatial coordinates in a given frame. In general, a spatial binning factor of 8 to 16 is used in order to result in images with sufficient contrast. The software allows defining regions of interest in the image, and it computes intensity time traces as well as nanotime histograms for each ROI.

In addition to representing the raw data of the H33D detector, the software computes a phasor for each photon. Using Eqns. (2.1) and (2.2), the nanotime value *t* for each single photon can be associated with a single-photon phasor coordinate (g_t, s_t) called a fundamental phasor. Because phasors add linearly, these fundamental phasors can be added just like intensity values to form G- and S-phasor "images", which, once normalized by the intensity image, provide the *g* and *s* phasor values for each pixel. This procedure allows extremely rapid generation of phasor data. The next section will describe how to obtain phasor plots and phasor ratio images from these data.

The H33D architecture is thus ideally suited to the generation of FLIM movies with almost no computational overhead.

3 RESULTS

3.1 Live cells with GFP and quantum dots

To demonstrate the capabilities of phasor analysis with the H33D, we reanalyzed previous live cell imaging data acquired with the H33D using the new phasor analysis routines. Briefly, HeLa cells expressing caveolin 1-EGFP and glycosylphosphatidylinisotol (GPI)-anchored avidin were labeled with non-biotinylated quantum dots emitting at 620 nm and observed using epifluorescence microscopy as described[7].
Fig. 5 shows the distribution of the two probes in the sample as shown by spectral separation of each probe's emission (same excitation at 442 nm). Fig. 5a shows the EGFP signal revealing the distribution of caveolin, while Fig. 5b shows the quantum dot signal, which appears to be largely concentrated near the nuclei. In Fig. 5c, the overlap of these two signals is shown.

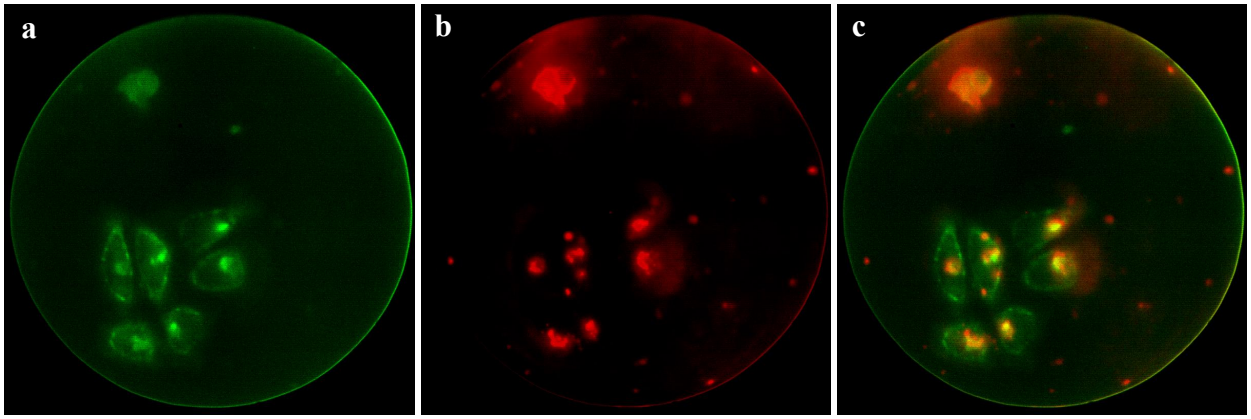

Fig. 5: HeLa cells measured with the H33D, using different emission filters. (a) 530DF30, (b) 615DF45, (c) 530DF30 as green overlapped with 615DF45 as red. Adapted from ref. [1]

Fig. 6a shows the color-coded intensity image of the same sample observed using a long pass filter (500LP), which allows the emission of EGFP, autofluorescence and quantum dots to be detected. In this figure, it is impossible to discern which areas actually corresponds to which probe since the spectral information has been lost. Fig. 6b shows the corresponding phasor ratio image, in which the blue color corresponds to a complex multiexponential phasor formed by EGFP combined with cell autofluorescence, while the red color corresponds to a multiexponential phasor given by the quantum dots. With this representation, it is easy to see the contrast between regions that are dominated by EGFP and regions that are dominated by quantum dot fluorescence. In particular, one recovers the membrane localization of the EGFP signal and the perinuclear localization of quantum dots observed in the spectrally separated images of Fig. 5c.

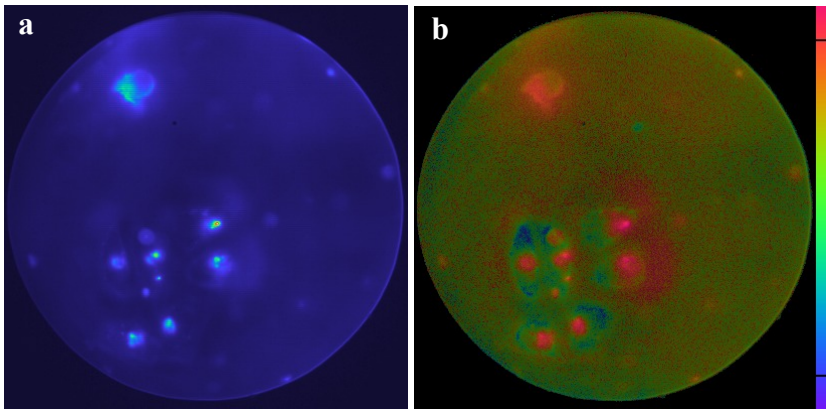

Fig. 6: H33D data of HeLa cells expressing caveolin 1-EGFP and GPI-anchored avidin labeled with non-biotinylated quantum dots emitting at 620 nm. (a) Intensity image. (b) The phasor ratio image, with the bottom hue representing GFP with autofluorescence, and the upper hue representing the quantum dots.

The phasor plot used to generate the phasor ratio image of Fig. 6b is shown in Fig. 7. The left side of the peak, at approximately $g = 0.3$, $s = 0.4$, corresponds to the quantum dot position, while the right side of the peak at approximately $g = 0.6$, $s = 0.2$, corresponds to the position given by EGFP combined with cell autofluorescence.

The same principle of operation demonstrated by this dataset could also be used with a FRET construct to display the ratio between binary FRET states, or with slight modification, to color an image based on a FRET value. These algorithms are also sufficiently rapid that they can be used to display a phasor ratio image and phasor plot during live acquisition.

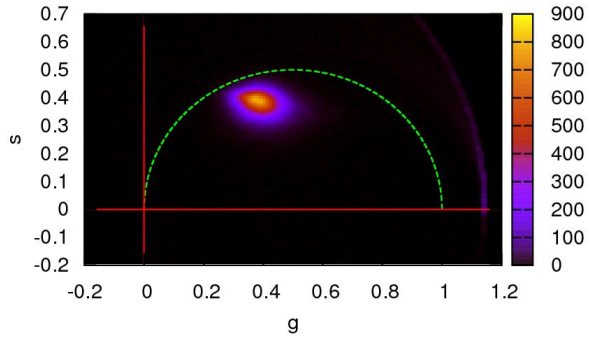

Fig. 7: The 19 MHz phasor plot for the data shown in Fig. 6, which shows the distribution of phasor values.

3.2 Single bead and quantum dot imaging

The application of phasor analysis to single molecules and point sources was demonstrated with measurements of 220 nm beads, shown in Fig. 8, and with quantum dots emitting at 577 nm, shown in Fig. 9. We applied an intensity threshold to the data to isolate only the phasors corresponding to pixels where the point sources are located, and plotted the resulting histogram of phasors in Fig. 8b and Fig. 9b respectively. In Fig. 8b, one can see the shorter lifetimes of the beads, in comparison to the longer quantum dot lifetimes in Fig. 9b. Note that for these point sources, there are fewer measurements histogrammed in the phasor plot than in Fig. 7, because the point sources occupy a much smaller number of pixels.

After identifying the region of the phasor plot corresponding to the probe of interest, one can isolate that probe in future measurements without performing any intensity thresholding. For example, if one has a single measurement containing both the beads and quantum dots shown here, then by selecting a region of interest on the phasor plot corresponding to the location of the phasors in Fig. 8b, then one can highlight only the pixels of the image containing beads with those lifetimes. With this approach, it should be possible to track point sources using a purely lifetime-based contrast and exploit this information to extract information on the probe's environment.

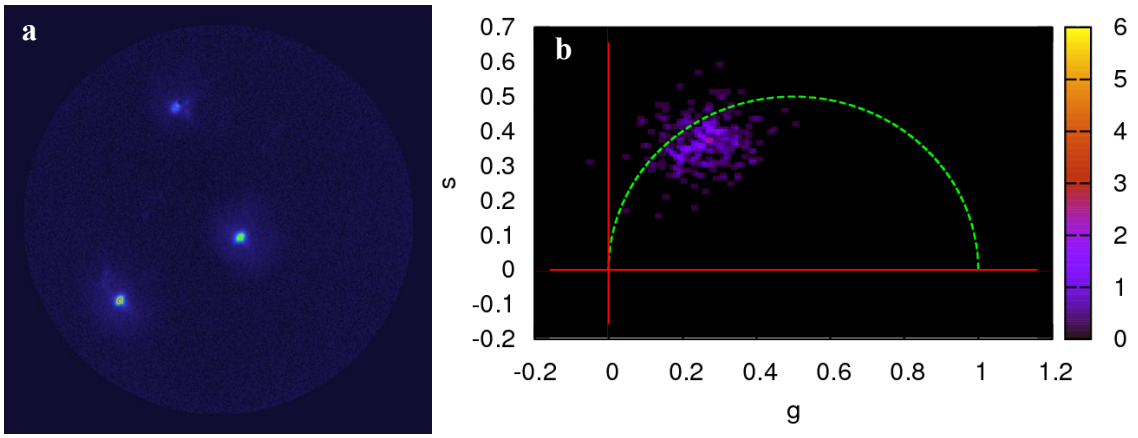

Fig. 8: H33D data showing (a) intensity images and (b) 68 MHz phasor plots for 220 nm nile red beads.

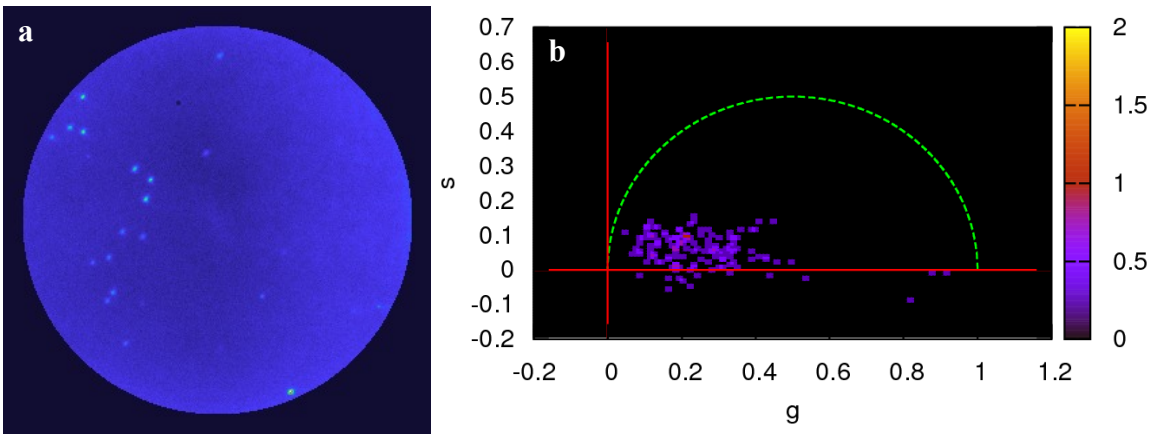

Fig. 9: H33D data showing (a) intensity images and (b) 68MHz phasor plots for 577 nm emitting CdSe/ZnS quantum dots.

4 DISCUSSION

4.1 Benefits of phasor analysis

We have demonstrated the combination of phasor analysis and the generation of phasor ratio images with the Gen 1 H33D detector. The application of this approach to data from the H33D detector provides a straightforward and rapid way to generate images with lifetime contrast as shown. The speed of phasor calculation makes it possible to calculate lifetime movies live during data acquisition. In addition, the linear nature of phasors allows one to arbitrarily rebin the stream of photons, yielding a lifetime image sequence at any frame-rate for which there are adequate counts.

The precision of a phasor coordinate improves with the square of the number of counts. Since the H33D detector provides a raw stream of photon counts, the phasor values can be rebinned in post-processing at different image resolutions and frame-rates, which will yield different numbers of photons per pixel and thus different phasor precision. The flexible nature of the H33D data stream means that data from a single acquisition can be examined with multiple priorities for spatial resolution, temporal resolution, and lifetime resolution.

4.2 Future development

Our current Gen. 1 H33D prototype is constrained to a maximum count rate of ~500 kHz (due to electronic limitations) and a local count rate of ~10 kHz (due to MCP saturation). We are currently developing a new version of the H33D detector comprising a number of improvements. In particular, use of a different position sensing anode (cross-strip anode[16]) will allow a reduction of the MCP gain while preserving the spatial resolution of the detector. This, in turn, will allow increasing the maximum local count rate to 100 kHz. The global count rate will also be improved to several MHz, thus enabling the simultaneous observation of millisecond dynamics across the entire image.

In addition, our next prototype will use a SuperGen II (S25) photocathode which offers a substantial increase in quantum efficiency compared to the current S20 photocathode, enabling single-molecule sensitivity for a wider range of probes.

With the demonstrations given here of the capabilities of this approach, we have shown that the development of this prototype and the methods described above are leading toward a wide-field photon-counting high-throughput FLIM system with single-molecule sensitivity and the simultaneous capability to observe millisecond dynamics across an entire image at once.

Acknowledgements

This work was supported by Grant NIH-BRG 5R01GM084327 and NSF-IDBR 0552099. We thank Dr. Pinaud for help with the preparation of the live cell samples.

References

[1] X. Michalet, O. H. W. Siegmund, J. V. Vallerga, P. Jelinsky, F. F. Pinaud, J. E. Millaud and S. Weiss, "Fluorescence lifetime microscopy with a time- and space-resolved single-photon counting detector", Proceedings of SPIE 6372, 63720E (2006).

[2] R. M. Clegg, [Fluorescence Imaging Spectroscopy and Microscopy], John Wiley & Sons: Hoboken (1996)

[3] K. Suhling, "Fluorescence lifetime imaging", [Cell Imaging], D. Stephens. Ed., Scion Publishing: Bloxham (2006)

[4] W. Becker, [Advanced time-correlated single photon couting techniques], Springer: Berlin (2005)

[5] R. A. Colyer, C. Lee and E. Gratton, "A novel fluorescence lifetime imaging system that optimizes photon efficiency", Microscopy Research and Technique 71, 201-213 (2008).

[6] E. B. van Munster, J. Goedhart, G. J. Kremers, E. M. M. Manders and T. W. J. Gadella, "Combination of a spinning disc confocal unit with frequency-domain fluorescence lifetime imaging microscopy", Cytometry 71A, 207-214 (2007).

[7] X. Michalet, O. H. W. Siegmund, J. V. Vallerga, P. Jelinsky, J. E. Millaud and S. Weiss, "A space- and time-resolved single-photon counting detector for fluorescence microscopy and spectroscopy", SPIE Proc. 6092, 60920M (2006).

[8] S. Pelet, M. J. R. Previte, L. H. Laiho and P. T. C. So, "A fast global fitting algorithm for fluorescence lifetime imaging microscopy based on image segmentation", Biophysical Journal 87, 2807-2817 (2004).

[9] D. M. Jameson, E. Gratton and R. D. Hall, "The Measurement and Analysis of Heterogeneous Emissions by Multifrequency Phase and Modulation Fluorometry", Applied Spectroscopy Reviews 20, 55-106 (1984).

[10] G. I. Redford and R. M. Clegg, "Polar plot representation for frequency-domain analysis of fluorescence lifetimes", Journal of Fluorescence 15, 805-815 (2005).

[11] A. H. A. Clayton, Q. S. Hanley and P. J. Verveer, "Graphical representation and multicomponent analysis of single-frequency fluorescence lifetime imaging microscopy data", Journal of Microscopy 213, 1-5 (2004).

[12] M. A. Digman, V. R. Caiolfa, M. Zamai and E. Gratton, "The phasor approach to fluorescence lifetime imaging analysis", Biophysical Journal 94, L14-L16 (2008).

[13] F. Pinaud, D. King, H. P. Moore and S. Weiss, "Bioactivation and cell targeting of semiconductor CdSe/ZnS nanocrystals with phytochelatin-related peptides", Journal of the American Chemical Society 126, 6115-6123 (2004).

[14] X. Michalet, O. H. W. Siegmund, J. V. Vallerga, P. Jelinsky, J. E. Millaud and S. Weiss, "Detectors for single-molecule fluorescence imaging and spectroscopy", J. Mod. Opt. 54, 239-282 (2007).

[15] X. Michalet, O. H. W. Siegmund, J. V. Vallerga, P. N. Jelinsky, J. E. Millaud and S. Weiss, "Photon-Counting H33D Detector for Biological Fluorescence Imaging", Nucl. Instrum. & Meth. A 567, 133-136 (2006).

[16] O. H. W. Siegmund, X. Michalet, J. V. Vallerga, P. Jelinsky and S. Weiss, "Cross delay line detectors for high time resolution astronomical polarimetry and biological fluorescence imaging", IEEE Nuclear Symposium Conference Record N14-55, 448-452 (2005).